

Segmentation of Airways Based on Gradient Vector Flow

Christian Bauer^{1,2}, Horst Bischof¹, and Reinhard Beichel^{2,3,4}

¹ Inst. for Computer Graphics and Vision, Graz University of Technology, Austria

² Dept. of Electrical and Computer Engineering

³ Dept. of Internal Medicine

⁴ The Iowa Institute for Biomedical Imaging

The University of Iowa, Iowa City, IA 52242, USA

{cbauer, bischof}@icg.tu-graz.ac.at

reinhard-beichel@uiowa.edu

Abstract. We present an automated approach for the segmentation of airways in CT datasets. The approach utilizes the Gradient Vector Flow and consists of two main processing steps. Initially, airway-like structures are identified and their centerlines are extracted. These centerlines are used in a second step to initialize the actual segmentation of the corresponding airways. An evaluation on 20 clinical datasets shows that our method achieves a good average airway branch count (63.0%) without any major leakage.

1 Introduction

Segmentation of airway trees in CT is of importance for various clinical applications, and several methods have been presented in the literature for this task. An overview can be found in the survey of Sluimer et al. [1]. A summary of newer approaches can be found in [2]. While some methods focus on accurate segmentation of airways, others are primarily targeting the extraction of airway tree skeletons that are of importance for applications like virtual bronchoscopy [3] or airway tree labeling and anatomical matching [4].

In our previous works [5, 6], we presented a generic framework for the direct extraction of complete curve skeletons of branched tubular structures from gray-value images. The approach utilizes the Gradient Vector Flow (GVF) [7] – an anisotropic edge preserving gradient diffusion method – to detect tubular objects [5] and to extract their associated medial curves [6]. It does not require a prior segmentation and extracts curve skeletons of comparable quality to sophisticated skeletonization methods applied to segmentations.

The GVF – that represents a core component of the approach – was originally presented to guide snake based segmentations [7]. In the literature, properties of the GVF (or similar gradient diffusion methods) have also been used differently, for example to generate voxel accurate 2D and 3D segmentations without using snakes [8–11], and issues related to initialization of the segmentation or deficiencies of the GVF in case of boundary concavities, as they would occur with

side branches in branched tubular networks, have been addressed. For example, Li et al. [11] used a gradient flow tracking in the GVF field in combination with a locally adaptive thresholding scheme based on gray value statistics to segment blob like 3D structures. To our knowledge, none of the so far presented methods is directly applicable for segmentation of tubular structures like airways.

In this work, we adapt our method such that an explicit segmentation is derived and utilize it to automatically segment airway trees in CT data. The method is generally applicable and may also be used in other application domains. For evaluation of our approach, the airway trees in 20 clinical lung CT datasets were segmented and evaluation results are reported.

2 Method

Our method consists of two main steps. First, centerlines of tubular objects are extracted. Second, the tubular structures associated with these centerlines are segmented. Intermediate processing results are depicted in Figs. 2, 3, and 4; appropriate masks were used for better visualization of some intermediate results.

2.1 Gradient Vector Flow

Our method is based on the Gradient Vector Flow (GVF) [7] – an edge preserving gradient vector diffusion function – and specifically requires an appropriate initial vector field where the vectors point towards the center of the structures of interest (airways) and whose magnitude reflects an edge-likeness (Fig. 1(b)). Therefore, the inverted local derivatives $F = -\nabla(G_\sigma \star I)$ are computed and normalized $F^n(\mathbf{x}) = \frac{F(\mathbf{x})}{|F(\mathbf{x})|} \frac{\min(|F(\mathbf{x})|, F_{max})}{F_{max}}$ for every voxel $\mathbf{x} = \{x, y, z\}$, where I is the original image and G_σ is a Gaussian filter kernel at scale σ . σ and F_{max} are application specific parameters reflecting the noise level and the expected contrast.

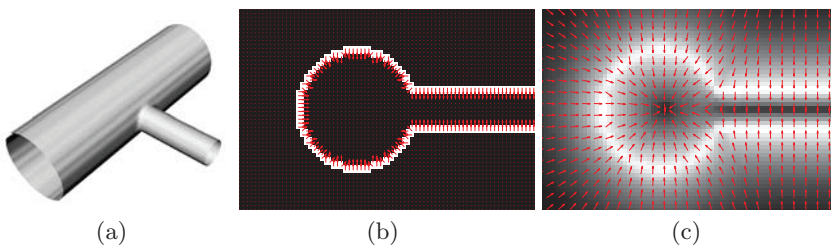


Fig. 1. Illustration of the GVF using a 2D cross section of a 3D branching tubular structure. (a) Branching 3D tubular structure. (b) Initial vector field $F^n(\mathbf{x})$ (gray-value: vector magnitude; arrow: vector direction). (c) Resulting GVF field $V(\mathbf{x})$ (gray-value: vector magnitude; arrow: vector direction).

Given this initial vector field $F^n(\mathbf{x})$, the GVF is calculated which is defined as the vector field $V(\mathbf{x})$ that minimizes:

$$E(V) = \iiint_{\Omega} \mu |\nabla V(\mathbf{x})|^2 + |F^n(\mathbf{x})|^2 |V(\mathbf{x}) - F^n(\mathbf{x})|^2 d\mathbf{x} \quad (1)$$

where μ is a regularization parameter. The variational formulation of the GVF keeps vectors with large magnitude nearly equal, while it produces a slowly varying field in areas with small vector magnitude. An initial vector field $F^n(\mathbf{x})$ and the GVF result $V(\mathbf{x})$ are shown in Figs. 1(b) and (c), respectively. For tubular objects, some characteristic properties can be observed. All vectors point from the boundary toward the center of the tubular objects where the vectors “collide”. The vector field shows a large variation in the cross-sectional planes of the tubular objects, but almost no variation along the tubes tangent direction. In addition, the magnitudes of the vectors show a medialness property: their values decreases with increasing distance from boundaries. At the centers of the tubular objects, the magnitude almost vanishes (it not necessarily becomes zero) and forms local directional minima. Examples of the initial and the GVF vector fields for a CT dataset are shown in Fig. 2. Below we will refer to the GVF field’s normalized direction as $V^n(\mathbf{x}) = V(\mathbf{x})/|V(\mathbf{x})|$ and to its magnitude as $M(\mathbf{x}) = |V(\mathbf{x})|$.

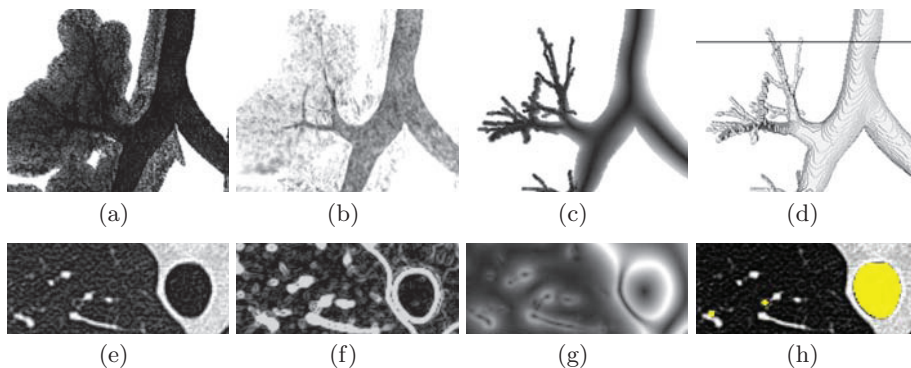


Fig. 2. Example showing some properties of the initial and the GVF’s vector fields magnitudes on a real dataset. (a) Minimum Intensity Projection (MinIP) of the dataset. (b) MinIP showing the Gauss-smoothed dataset with $\sigma = 0.5$ that was used to calculate the initial gradient $F(\mathbf{x})$. (c) MinIP of the GVF magnitude $M(\mathbf{x})$ inside the segmentation result. (d) Segmentation result; the axial cutting plane used in (e)-(h) is indicated by a black line. (e) Axial slice of the dataset showing part of the trachea and some thin low contrast airways. (f) Magnitude of initial vector field $|F^n(\mathbf{x})|$ before applying the GVF. (g) Magnitude $M(\mathbf{x})$ of the GVF field. (h) Segmentation result.

In the following sections, we will show how we utilize these properties for airway centerline extraction and segmentation.

2.2 Tube Centerline Extraction

To identify tubular objects and to extract their centerlines, the Hessian matrix $H(\mathbf{x}) = \nabla V(\mathbf{x})$ with its eigenvalues $|\lambda_1| \leq |\lambda_2| \leq |\lambda_3|$ and eigenvectors \mathbf{v}_1 , \mathbf{v}_2 , and \mathbf{v}_3 is computed for all voxels in the image to obtain the tubes cross-sectional plane spanned by \mathbf{v}_2 and \mathbf{v}_3 . Based on this information, center points are identified as local directional minima in the medialness map M . In this way, center points (colored points in Fig. 3(a)). To identify those center points that are related to tubular objects, a tube-likeness $T(\mathbf{x})$ is computed. For this purpose, a circle is fitted to the data in the tubes cross-sectional plane. The quality of the fitting determines the tube-likeness. Compared to using a weighting of the eigenvalues of the Hessian matrix to determine a tube-likeness [5, 6], this allows for a higher selectivity. The fitting term [12] is computed as the mean flow through the circle and depends on the radius r : $T(\mathbf{x}, r) = \frac{1}{2r\pi} \int_{\alpha=0}^{2\pi} \langle V(\alpha, r), D(\alpha) \rangle d\alpha$. $V(\alpha, r)$ represents the GVF's vector at the circle point and $D(\alpha)$ defines a normal vector on the circle pointing towards its center. The integral is approximated by computing the sum over 32 discrete circle points. During the circle fitting procedure, the radius is steadily increased until the circle touches an actual edge/surface of the object. Increasing r further results in a drop of $T(\mathbf{x}, r)$ as the magnitude of the vectors drop off. Thus, the fitting is performed for increasing radii as long as the fitting term increases. The best fit determines the tube-likeness $T(\mathbf{x})$.

Applying this procedure to the GVF field results in a tube-likeness measure at the centerlines, as shown in Fig. 3(b). This information can be used for detection and centerline extraction of tubular objects. However, for thin low contrast airways, the response may fall off strongly, if their gradient-magnitude is too low so that they are not completely preserved in the GVF result (Figs. 2(f) and (g)). Applying the same procedure with a radius of $0.5mm$ on the initial vector field $F^n(\mathbf{x})$ allows identification of these structures as shown in Fig. 3(b), and therefore, the maximum of both responses is utilized to produce a combined tube-likeness volume. To extract the centerlines and to discard non-tubular objects, a hysteresis thresholding with t_h and t_l is performed on the tube-likeness volume and neighboring centerline points are linked together into centerlines. From these initial centerlines, short spurious centerlines with a length (below t_s) are discarded. In addition, centerlines with a mean tube-likeness below t_m are removed. The resulting centerlines of the tubular objects are shown in Fig. 3(c).

2.3 Inverse Gradient Flow Tracking Tube Segmentation

After extraction of the airway centerlines, the associated image regions are segmented. In the GVF field, the vectors flow towards the centers of the airways, which correspond to the extracted centerlines (in case of tubular objects). By following the direction of the gradient vectors, each voxel can be assigned to a neighboring voxel and a path can be tracked for each voxel of the airway to its centerline. Based on this assignment and the fact that the gradient magnitude increases until the actual boundary is reached, the airways associated with the

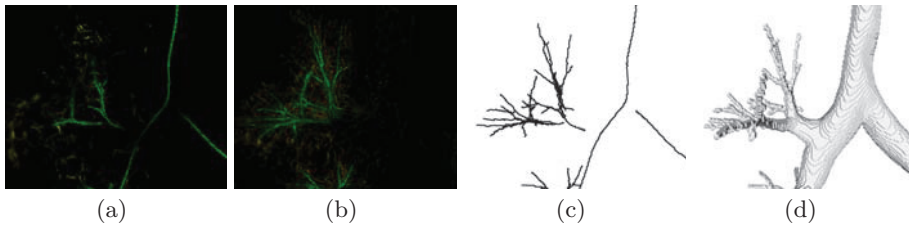


Fig. 3. Intermediate results of the tube centerline extraction method. The tube likeliness for the computed centerline points is shown as intensity value, and the extracted centerlines are drawn in green. (a) Tube-likeness for larger structures. (b) Tube-likeness for thin low contrast structures. (c) Extracted tube centerlines. (d) Segmentation result showing the size of the airways.

individual centerlines are segmented by following the gradient flow tracking path in the inverse direction. Starting from the points at the tubes center, neighboring voxels fulfilling these criteria are merged iteratively to generate a segmentation (Algorithm 1).

Algorithm 1 Inverse gradient flow tracking tube segmentation

```

input: GVF field  $V(x)$  with direction  $V^n(x)$  and magnitude  $M(x)$ 
input: centerline points  $C = \{x_1, x_2, \dots, x_n\}$ 
set  $S \leftarrow C$ 
queue  $Q \leftarrow C$ 
while  $Q \neq \{\}$  do
   $x \leftarrow \text{extract}(Q)$ 
  for each voxel  $y \in \text{Adj26}(x)$  do
    if  $y \notin S$  and  $M(y) > M(x)$  and  $\text{argmin}_{z \in \text{Adj26}(y)} \langle V^n(y), \vec{y-z} \rangle = x$  then
       $S \leftarrow S \cup \{x\}$ 
       $Q \leftarrow Q \cup \{y\}$ 
    end if
  end for
end while
output: segmented tube voxels  $S$ 

```

Examples of segmented airway branches assigned to individual centerlines generated with this algorithm are shown in Fig. 4. Note that the individually segmented parts do not “leak” into side branches of the airway tree, and the combination of all individually segmented airway branches provides a valid segmentation of the complete airway tree. Another example segmentation is shown in Fig. 2(h) where the segmentation of thin low contrast airways is clearly visible.

To discard non-airway structures and to assure a 6-connected segmentation result, the following post-processing was applied to the datasets. The extracted centerlines were dilated and added to the segmentation result to assure

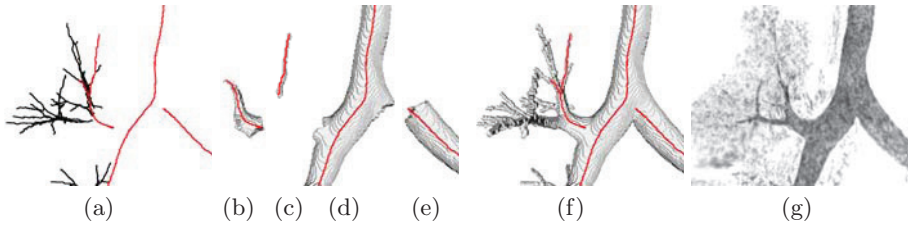


Fig. 4. Illustration of the inverse gradient flow tracking tube segmentation. (a) Extracted centerlines showing 4 selected centerlines. (b)-(e) Segmentations associated with the selected centerlines. (f) Combined results of all tubular structures. (h) MinIP of smoothed dataset for comparison.

6-connectivity. The actual airway tree was identified as the largest connected segmented component and other segmented tubular structures were discarded.

3 Evaluation

The approach was applied to 40 clinical CT datasets of the thorax (undisclosed reference segmentations) which were provided by the organizers of the “Extraction of Airways from CT 2009 (EXACT09)” workshop. The datasets were split into two sets of 20 training datasets where parameters were adapted and 20 testing datasets. The following set of parameters was used for segmentation of all 40 datasets: $\sigma = 0.5$, $F_{max} = 200$, $\mu = 5$, $t_h = 0.5$, $t_l = 0.1$, $t_s = 5$, and $t_m = 0.5$. The GVF was computed using an iterative update scheme with 500 iterations [7]. The segmentation results were sent to the organizers, who in return provided evaluation results for the 20 test cases (see Table 1). For information about how the reference segmentations were obtained and the exact definition of the used performance measures we refer to <http://image.diku.dk/exact/information.php>. On average, 63.0% of airway branches were detected with an average detected tree length of 58.4%. The mean leakage count was 5.0, and the mean false positive rate was 1.44% (median: 0.61%).

4 Discussion

The evaluation results show that our method achieves a good average airway branch count (63.0%) without any major leakage. One exception is CASE39, where some leakage occurred ($3577mm^3$).

In the following, we discuss some properties of our approach. Examples of segmentation results are shown in Fig. 5 and Fig. 6. As can be seen, the segmented surface shows a good correspondence with the image data. The tube detection/segmentation method is also capable of handling cases where the airway shape deviates from a perfectly circular or purely convex shape (e.g., trachea

Table 1. Evaluation results on the twenty test cases.

	Branch count	Branch detected (%)	Tree length (cm)	Tree length detected (%)	Leakage count	Leakage volume (mm ³)	False positive rate (%)
CASE21	114	57.3	68.5	62.0	3	35.2	0.31
CASE22	270	69.8	218.9	66.2	9	474.6	1.60
CASE23	187	65.8	134.0	51.5	5	43.5	0.20
CASE24	139	74.7	113.9	70.0	8	176.9	0.59
CASE25	158	67.5	123.1	48.8	4	98.6	0.32
CASE26	59	73.8	51.2	78.0	2	274.3	2.70
CASE27	77	76.2	58.1	71.7	4	353.5	3.06
CASE28	86	69.9	66.9	61.0	1	49.6	0.43
CASE29	120	65.2	81.2	58.8	4	118.9	0.85
CASE30	114	58.5	87.5	57.2	5	98.9	0.64
CASE31	96	44.9	70.5	40.2	1	59.8	0.34
CASE32	101	43.3	80.3	36.8	1	175.2	0.86
CASE33	117	69.6	90.4	61.5	1	32.0	0.29
CASE34	250	54.6	184.6	51.6	11	358.1	1.05
CASE35	168	48.8	110.9	35.9	5	69.8	0.30
CASE36	294	80.8	330.6	80.2	5	78.6	0.25
CASE37	112	60.5	87.9	49.5	2	102.9	0.48
CASE38	64	65.3	51.2	77.1	4	311.0	2.64
CASE39	291	56.0	250.6	61.2	13	3577.0	9.21
CASE40	225	57.8	187.7	48.5	11	959.0	2.65
Mean	152.1	63.0	122.4	58.4	5.0	372.4	1.44
Std. dev.	75.7	10.4	75.2	13.2	3.6	785.4	2.06
Min	59	43.3	51.2	35.9	1	32.0	0.20
1st quartile	96	56.0	68.5	48.8	2	59.8	0.31
Median	119	65.3	89.2	59.9	4	110.9	0.61
3rd quartile	250	73.8	187.7	71.7	9	358.1	2.65
Max	294	80.8	330.6	80.2	13	3577.0	9.21

of CASE18 in Figs. 5 and 6). Leakage into non-tubular structures is uncommon. However, in case of emphysema some leakage was observed (e.g., CASE14 in Fig. 5).

An additional advantage of our approach is that the presented centerline extraction method may be easily extended to extract the complete curve skeleton of the airway tree. This can be achieved by obtaining connections between the individual centerlines based on the GVF's medialness property as we showed in our previous work [6]. An example of the skeleton extracted with our method from the already computed GVF field is shown in Fig. 7(a). For comparison, we also extracted a skeleton with the skeletonization approach presented by Palagyi et al. [13] based on the binary segmentation obtained with our presented GVF segmentation approach. A comparison with other skeletonization approaches is provided in [6]. As can be seen, the skeleton extracted with our GVF based approach has high quality.

Regarding computation time, we utilize a GPU (graphics processing unit) implementation using the CUDA framework¹ for computation of the GVF. Other parts of the implementation are not optimized. On average, our algorithm requires 6 minutes for segmentation of the airways using an NVIDIA Tesla C1060 card processing the whole dataset. This time can be reduced to 2 minutes when the computation is restricted to an axis aligned subvolume surrounding the lung area.

5 Conclusion

In this work we presented an approach for the identification and segmentation of airway trees in CT data based on GVF. First, the method extracts centerlines of the airways. This information is then utilized in an inverse gradient flow tracking step for the actual segmentation of individual airways. In addition, the utilized GVF field may also be used for the extraction of a high quality skeleton.

6 Acknowledgments

This work was supported in part by the Austrian Science Fund (FWF) under the doctoral program Confluence of Vision and Graphics W1209 and the Austrian Marshall Plan Foundation.

References

1. Sluimer, I., Schilham, A., Prokop, M., van Ginneken, B.: Computer analysis of computed tomography scans of the lung: A survey. *IEEE Trans. Med. Imag.* **25**(4) (Apr. 2006) 385–405
2. Graham, M.W., Gibbs, J.D., Higgins, W.E.: Robust system for human airway-tree segmentation. In: *Proc. of SPIE Med. Imag.* (Mar. 2008)

¹ http://www.nvidia.com/object/cuda_home.html

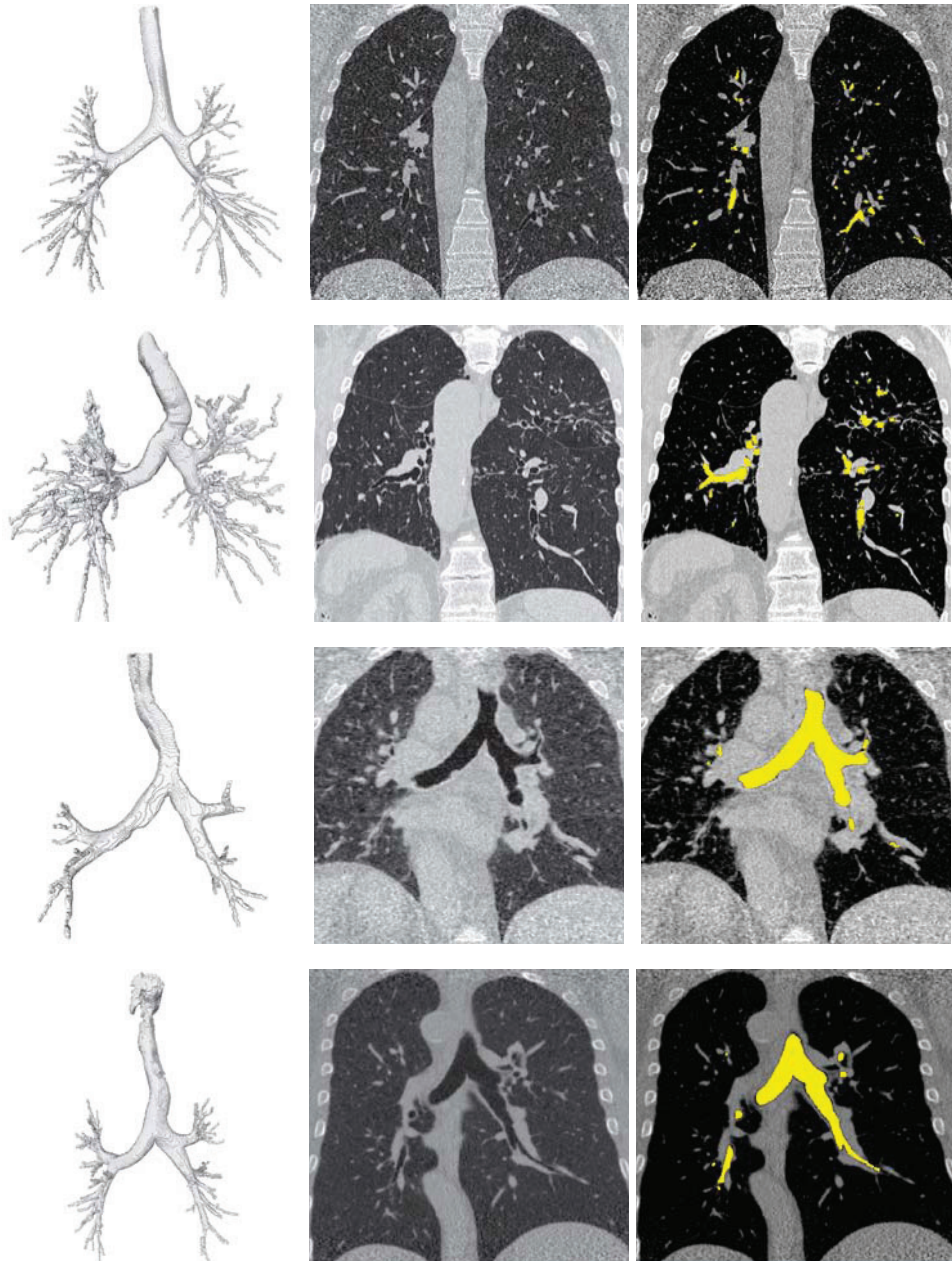


Fig. 5. Examples of segmentation results (EXACT09 database). From top to bottom: CASE03, CASE14, CASE18, CASE24. From left to right: 3D visualization of result; coronal slice showing CT data; coronal slice showing the segmentation result.

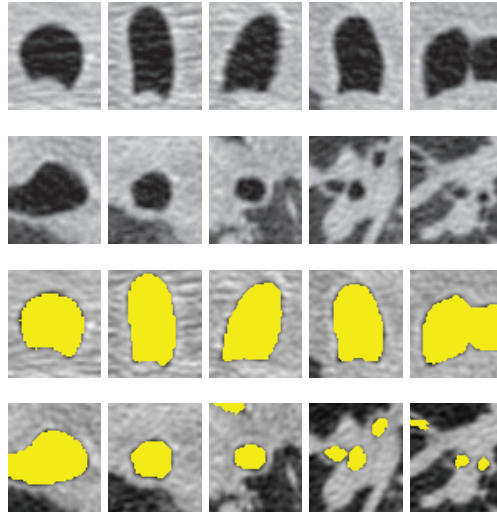


Fig. 6. Segmentation results in axial planes along a path from the root of the trachea to a distal end of an airway for a dataset where the cross-sectional profile deviates from a circular shape (CASE18; see also row 3 in Fig. 5). Note that for visualization of the CT datasets, a linear interpolation was used which resulted in a blurring of the image.

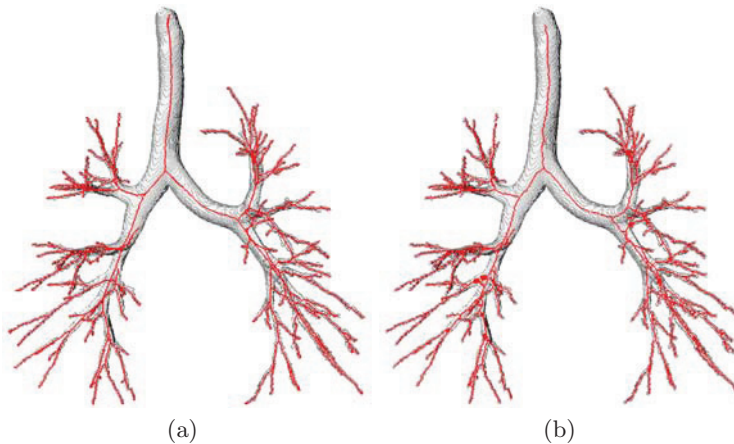


Fig. 7. Curve skeletons extracted with (a) our approach presented in [6] based on the already computed GVF field and (b) the skeletonization method presented in [13] based on the binary segmentation.

- Swift, R.D., Kiraly, A.P., Sherbondy, A.J., Austin, A.L., Hoffman, E.A., McLennan, G., Higgins, W.E.: Automatic axis generation for virtual bronchoscopic assessment of major airway obstructions. *Comput. Med. Imaging Graphics* **26**(2) (2002) 103 – 118

4. Tschirren, J., McLennan, G., Palágyi, K., Hoffman, E.A., Sonka, M.: Matching and anatomical labeling of human airway tree. *IEEE Trans. Med. Imag.* **24**(12) (Dec. 2005) 1540–1547
5. Bauer, C., Bischof, H.: A novel approach for detection of tubular objects and its application to medical image analysis. In: Proc. of DAGM. (2008) 163–172
6. Bauer, C., Bischof, H.: Extracting curve skeletons from gray value images for virtual endoscopy. In: Proc. of MIAR. (2008) 393–402
7. Xu, C., Prince, J.L.: Snakes, shapes, and gradient vector flow. *IEEE Trans. on Image Processing* **7**(3) (Mar. 1998) 359–369
8. Yu, Z., Bajaj, C., Bajaj, R.: Normalized gradient vector diffusion and image segmentation. In: Proc. of ECCV. (2002) 17–530
9. Chuang, C.H., Lie, W.N.: A downstream algorithm based on extended gradient vector flow field for object segmentation. *IEEE Trans. Med. Imag.* **13**(10) (Oct. 2004) 1379–1392
10. Schmutz, S.J., Keller, S., Nguyen, N., Souvenir, R., Huynh, T., Clemens, M., Shin, M.C.: Segmentation of vessels cluttered with cells using a physics based model. In: Proc. of MICCAI. (2008) 127–134
11. Li, G., Liu, T., Tarokh, A., Nie, J., Guo, L., Mara, A., Holley, S., Wong, S.: 3D cell nuclei segmentation based on gradient flow tracking. *BMC Cell Biology* **8**(40) (2007)
12. Krissian, K., Malandain, G., Ayache, N., Vaillant, R., Troussel, Y.: Model-based detection of tubular structures in 3D images. *CVIU* **2**(80) (2000) 130–171
13. Palágyi, K., Sorantin, E., Balogh, E., Kuba, A., Halmai, C., Erdohelyi, B., Hausegger, K.: A sequential 3D thinning algorithm and its medical applications. In: IPMI, Springer-Verlag Heidelberg (2001) 409–415